Journal of Applied Electrochemistry (2006) 36:789–800
DOI 10.1007/s10800-006-9139-6

Electrodeposition of Cu from acidic sulphate solutions in the presence of PEG: An electrochemical and spectroelectrochemical investigation – Part I

B. BOZZINI[1,*], C. MELE[1], L. D'URZO[1], G. GIOVANNELLI[2] and S. NATALI[2]
[1]*Dipartimento di Ingegneria dell'Innovazione, Università di Lecce, via Monteroni, I-73100, Lecce, Italy*
[2]*Dipartimento ICMMPM, Università di Roma "La Sapienza", v. Eudossiana 18, I-00184, Roma, Italy*
*(*author for correspondence, e-mail: benedetto.bozzini@unile.it)*

Received 14 April 2004; accepted in revised form 14 February 2005

Key words: copper, electrodeposition, PEG, SERS, ULSI fabrication

Abstract

This paper deals with the effects of PEG during Cu electrodeposition from an acidic sulphate solution. This investigation was carried out with electrochemical and spectroelectrochemical techniques. Potentiostatically grown layers were examined by scanning electron microscopy. Adsorption of PEG on the growing Cu surface can be inferred from electrokinetic, SERS and morphological evidence: variations of the estimated exchange current density, qualitative and quantitative differences in the potentiostatic transients, changes on the cathodic current efficiency, effects on the three-dimensional crystallisation mode under both compact and dendritic growth conditions, appearance of surface-enhanced PEG-related Raman bands. SERS spectra revealed cathodic reactivity of adsorbed PEG.

1. Introduction

The mechanism of the electrodeposition of Cu from Cu^{2+} acidic sulphate baths has been comprehensively investigated [1]. The electrokinetic effects of Cl^- in acidic sulphate baths have also been extensively studied [2–5]. Interest in this system has recently been revived in relation to the fabrication of semiconductor devices. This process relies heavily on the use of complex blends of organics, whose action has been the objective of much research; this has, however not entirely unravelled the characteristics of these systems. The molecular-level understanding of these systems is still limited, as the main emphasis has been on the achievement of optimal filling properties and engineering management of the process.

Several experimental approaches have been used in order to differentiate the effects of the relevant organic species, but *in situ* spectroelectrochemistry has received surprisingly limited attention. The authors are aware of only few papers dealing with SERS during the electrodeposition of Cu both in the absence [6] and presence of organic additives [7, 8].

In this paper we focus on the effects of PEG $H(OCH_2CH_2)_nOH$ on the Cu electrodeposition process, as part of a more extensive investigation of the action of additives composing a typical cocktail empirically found to be effective in feature filling relevant to the semiconductor industry. We report some electrochemical (cyclic voltammetry with a rotating disk electrode, potentiostatic transients), spectroelectrochemical (*in situ* surface-enhanced Raman spectroscopy, SERS) and morphological (scanning electron microscopy, SEM) investigations of the effects of PEG during the electrodeposition of Cu from a conventional acidic sulphate electrolyte.

PEG is characterised by monomer units $–O–CH_2–CH_2–$ containing one hydrophobic moiety $–CH_2–CH_2–$ and one hydrogen bonding site –O–. The presence of electron-rich O atoms in the polymer backbone provides an available site for coordination with metallic species due to the interaction of the electron shells of O and metal cations, adcations or adatoms. Anions do not interact directly with PEG, but they can do so indirectly through coordinated cations. Cu^{2+} and Cu^+ exhibit a mild acidity and tend to interact weakly with oxygen-containing compounds. Nevertheless PEG is a polymer with strong surface active properties, allowing the formation of mono- and multilayers on metallic surfaces [9–25]. As far as the effects of PEG during Cu electrodeposition are concerned, this molecule is generally believed to give rise to a marked overpotential increase during electrodeposition of Cu from acidic sulphate solutions containing Cl^-, owing to adsorption at the growing cathode [9–13].

2. Experimental

The electrodeposition bath was: $CuSO_4{\cdot}5H_2O$ 20 mM, H_2SO_4 0.5 M. To this solution NaCl 500 ppm and/or PEG MW 1500, 2 g l^{-1} were added. We used analytical grade chemicals and ultra-pure water with a resistivity of 18.2 MΩ cm from a Millipore-Milli-Q system. The solutions were degassed by N_2 bubbling and maintaining the solution under a N_2 blanket during the measurements. To minimise organic contamination, all the items in contact with the working electrolyte were rinsed with concentrated HNO_3 before and after each experiment and stored in 20 vol% HNO_3 diluted with ultra-pure water.

Electrochemical measurements were performed with an AMEL 5000 programmable potentiostat and a three-electrode cylindrical cell. A PAR Model 636 rotating-disk electrode (RDE) was used. The working electrode (WE) was a PAR Pt rotating disk of 4 mm diameter. Rotation rates in the range 250–1750 rpm were adopted. The CVs were measured at a scan rate of 10 mV s^{-1}. The counter electrode (CE) was a platinised Ti mesh electrode 10 cm^2 in area. The reference electrode (RE) was an AMEL Ag/AgCl containing a 3 M KCl separated from the electroplating solution by a porous ceramic insert. The RE tip was placed at a distance of 5 mm from the WE rim. Ohmic corrections applied by the positive feedback method were considered, but proved irrelevant due to the high conductivity of the solution. Voltages are reported against Ag/AgCl.

Current efficiency measurements were carried out galvanostatically in an undivided prismatic plane-parallel electrode cell containing 1 l of electrolyte. The electrodes were either Cu foils (cathode and soluble anode) or a platinised Ti expanded-mesh (insoluble anode). The electrode area was in all cases 100 cm^2.

SERS measurements were performed with a LabRam confocal Raman system. Excitation at 633 nm was provided by a 12 mW He–Ne laser. A 50× long-working-distance objective was used. *In situ* spectro-electrochemistry was carried out in a cell with a vertical polycrystalline Cu disc WE of diameter 5 mm embedded in a Teflon cylindrical holder. A metallographic polishing procedure, consisting of wet grinding with 2400 grit SiC paper, allowed excellent reproducibility. The CE was a Pt wire loop (1.25 cm^2) concentric and coplanar with the WE disc. The RE was placed in a separate compartment. The RE probe tip was placed 3 mm from the rim of the working electrode disc. Raman intensities are normalised over the acquisition time and proportional to the discharge current of the CDD element corresponding to a given Raman shift, uncorrected for quantum efficiency.

A Cambridge Stereoscan 360 SEM was used. The electron source was LaB_6. Electron detection was carried out with a scintillation photodetector. The typical working pressure was 10^{-7} mbar.

3. Results and discussion

3.1. *Electrochemical measurements*

3.1.1. *Cyclic voltammetry*

CV curves for Cu electrodeposition were measured in the pure sulphate bath (Figure 1), with added PEG (Figure 2) and in the presence of both PEG and Cl^- (Figure 3). CVs are performed in the potential range: +750 to −750 mV. For each bath three replicas including two CV cycles each were run. The cycles started and finished at anodic potentials in order to restore the initial electrodic conditions at the beginning of each measurement.

By inspection of the cathodic going scan of the CV curves, a Tafel-type growth followed by a limiting current density (c.d.) can be observed. At more cathodic potentials, a second Tafel-type growth starts, corresponding to the onset of hydrogen evolution and PEG reaction. Details of the cathodic behaviour of PEG, which are not addressed in this paper for reasons of space, give rise to a small loop at the higher cathodic potentials. The anodic going scan crosses the forwards scan giving rise to a nucleation loop and eventually an anodic stripping peak is observed.

With the addition of PEG, the anodic curve is shifted to higher potentials because of a filming effect, giving rise to some degree of corrosion inhibition. In the solution without PEG, the growing portion of the anodic curve is not affected by the rotation rate, denoting a purely charge-transfer controlled process. On the contrary, in the presence of PEG, denobling correlates with rotation rate, probably owing to detachment of the PEG film. In the solution containing PEG and Cl^-, a double stripping peak can be noticed, which

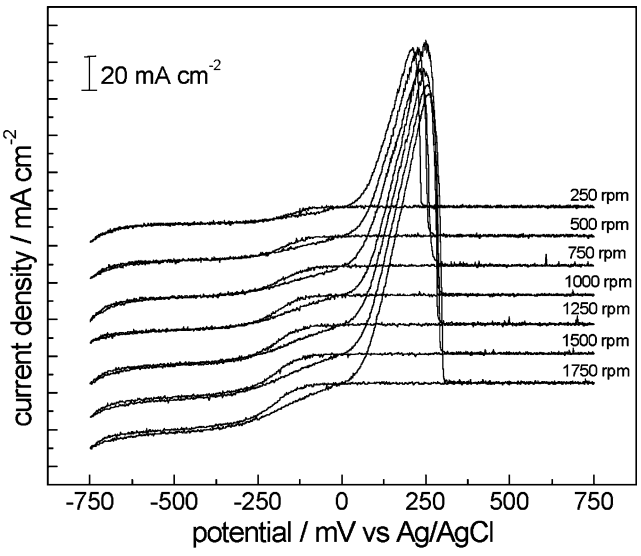

Fig. 1. Cyclic voltammograms for Cu electrodeposition from a bath containing $CuSO_4{\cdot}5H_2O$ 20 mM and H_2SO_4 0.5 M, for rotation rates from 250 to 1750 rpm. Working electrode: Pt disk. Scan rate: 10 mV s^{-1}.

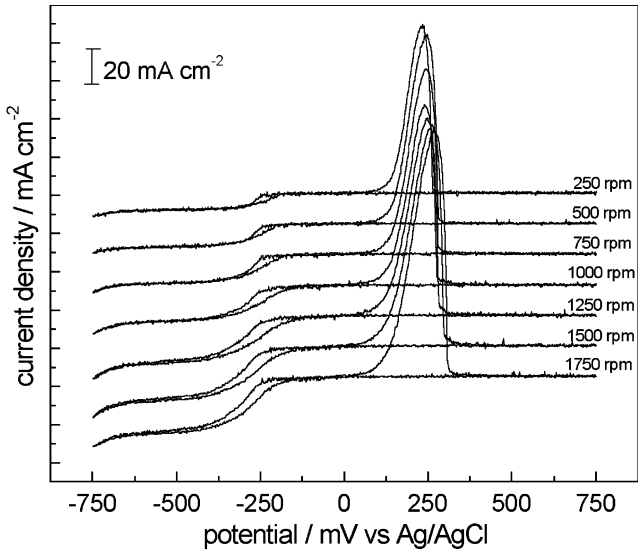

Fig. 2. Cyclic voltammograms for Cu electrodeposition in a bath containing $CuSO_4{\cdot}5H_2O$ 20 mM, H_2SO_4 0.5 M and PEG MW 1500 2 g l^{-1}, for rotation rates from 250 to 1750 rpm. Working electrode: Pt disk. Scan rate: 10 mV s^{-1}.

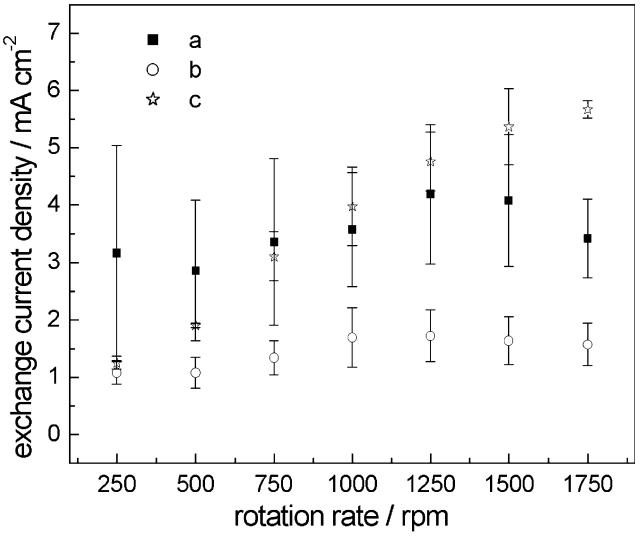

Fig. 4. Exchange current density ±1SD, estimated from the Butler-Volmer model (see Sect. 1.1), as a function of the RDE electrode rate for the solutions: (a) $CuSO_4{\cdot}5H_2O$ 20 mM and H_2SO_4 0.5 M, (b) $CuSO_4{\cdot}5H_2O$ 20 mM, H_2SO_4 0.5 M and PEG MW 1500 2 g l^{-1}, (c) $CuSO_4{\cdot}5H_2$ O 20 mM, H_2SO_4 0.5 M PEG MW 1500 2 g l^{-1} and NaCl 500 ppm.

can be related to the formation of Cu^+–Cl^- complexes [5].

The CVs were analysed numerically with a Butler-Volmer model and allowing for a limiting c.d. [26]. The parameters obtained by non-linear least-squares fitting were the exchange c.d. j_0, the anodic and cathodic Tafel slopes β_a and β_c, the limiting c.d. j_{lim} and the immersion potential V_o. The parameter estimates and their 95% confidence intervals, evaluated from the three replicated runs, are reported v the RDE rotation rate in Figures 4–7.

The presence of PEG, independently from the presence of Cl^-, results in a decrease of the activity of Cu^{2+} (see Figure 7). The exchange c.d. is higher in the presence of PEG (Figure 4); this can be explained with the fact that adsorbed PEG interacts strongly with the Cu surface.

As far as the cathodic Tafel slopes are concerned, some literature information exists on alterations brought about by the addition of PEG [13], but there is no quantitative discussion of these data. The analysis of our data shows that the cathodic Tafel slope decreases in the presence of PEG (Figure 5), denoting an enhancement of the charge transfer rate. Similar non-trivial results were obtained in the presence of different

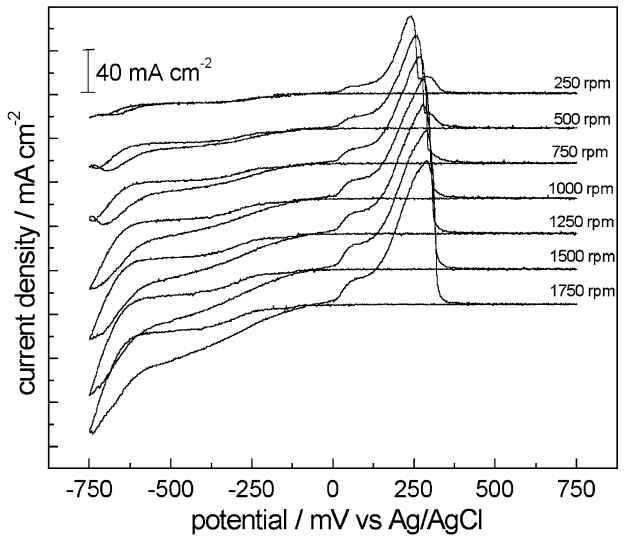

Fig. 3. Cyclic voltammograms for Cu electrodeposition in a bath containing $CuSO_4{\cdot}5H_2O$ 20 mM, $H_2SO_4$0.5 M, PEG MW 1500 2 g l^{-1} and NaCl 500 ppm, for rotation rates from 250 to 1750 rpm. Working electrode: Pt disk. Scan rate: 10 mV s^{-1}.

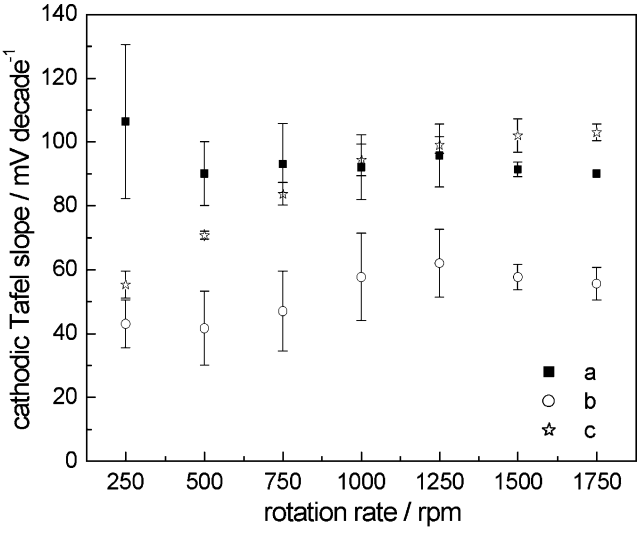

Fig. 5. Cathodic Tafel slopes ±1SD, estimated from the Butler-Volmer model (see Section 1.1), as a function of the RDE electrode rate for the solutions: (a) $CuSO_4{\cdot}5H_2O$ 20 mM and H_2SO_4 0.5 M, (b) $CuSO_4{\cdot}5H_2O$ 20 mM, H_2SO_4 0.5 M and PEG MW 1500 2 g l^{-1}, (c) $CuSO_4{\cdot}5H_2O$ 20 mM, H_2SO_4 0.5 M PEG MW 1500 2 g l^{-1} and NaCl 500 ppm.

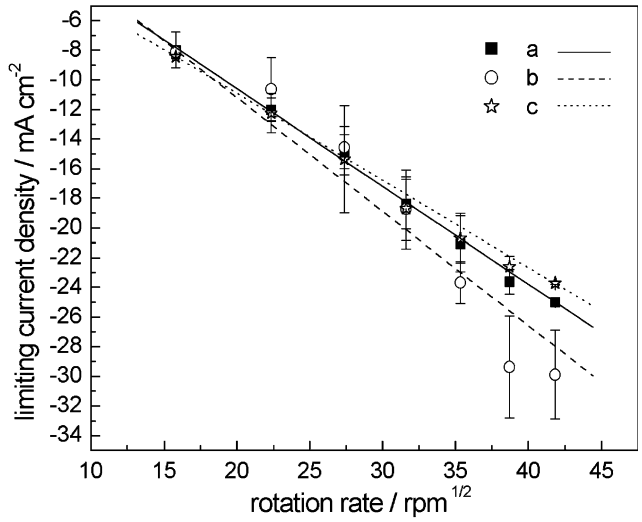

Fig. 6. Limiting current density ±1SD, estimated from the Butler-Volmer model (see Section 1.1), as a function of the RDE electrode rate for the solutions: (a) $CuSO_4{\cdot}5H_2O$ 20 mM and H_2SO_4 0.5 M, (b) $CuSO_4{\cdot}5H_2O$ 20 mM, H_2SO_4 0.5 M and PEG MW 1500 2 g l^{-1}, (c) $CuSO_4{\cdot}5H_2O$ 20 mM, H_2SO_4 0.5 M PEG MW 1500 2 g l^{-1} and NaCl 500 ppm. The lines represent fits with the Levich equation.

organics in electrodeposition studies from acidic sulphate solutions [27]. Charge-transfer enhancement was explained with an ion-bridging mechanism implying the ability of a complexed ion to accelerate the rate of electron transfer from the electrode to the metal ion through the additive [28, 29]. The relative rate increase with respect to the condition without additive is due to the fact that no electron transfer occurs through the primary water molecules bound to the electroactive ion.

For the solution containing PEG and Cl^-, β_c is still higher; this can be interpreted as due to an increase of resistance to electron transfer due to the mode of adsorption of Cl^-, which is expected to be positioned between PEG and metal surface [30]. In the presence of Cl^-, on increasing the rotation rate, the values of j_0 and β_c change from those characteristic for PEG-containing solutions towards those for PEG-free solutions. Since complexes between Cu^{2+} and Cl^- are expected to form in this solution, the surface concentration of Cl^- is increased upon reduction of Cu^{2+}, owing to ligand release. Therefore, metastably adsorbed Cl^- is expected also for potentials more cathodic then the point of zero charge (PZC) (about −200 mV [31]). A similar behaviour was demonstrated for pseudohalides under cognate electrochemical conditions [32]. The cathodic surface concentration is expected to be enhanced by reduction and mass-transport rates. On increasing of the amount of surface Cl^-, the scenario tends to become similar to that of the system without PEG. In fact, the formation of a surface ion-couple giving rise to the adsorption of PEG mediated by Cl^-, brings about the loss of electron transfer enhancement.

The cathodic region of the CV curves exhibits a nucleation loop. For the solution without PEG, the onset of this loop is at about 0 mV. For the solutions containing PEG and both PEG and Cl^-, the nucleation loop starts at more cathodic potential (−100 mV). The nucleation overpotential is ca. 100 mV, irrespective of the composition of the solutions.

The expected Levich behaviour of the limiting c.d. vs the square rate of rotation rate is found in our data (Figure 6), linear correlation coefficient in excess of 98% were always found. From these plots the diffusion coefficient for the cupric ions can be estimated by means of the Levich equation, assuming for the solution the viscosity value of water. The variations of solution viscosity with PEG are expected to be limited and the quantitative impact on the evaluation of the diffusion coefficient is still mitigated by the small exponent. For the solutions without PEG, with PEG and with both PEG and Cl^-, the following values of the diffusion coefficient are found, respectively: $5.89 \pm 0.01 \times 10^{-6}$ cm^2 s^{-1}, $7.41 \pm 0.06 \times 10^{-6}$ cm^2 s^{-1}, and $5.22 \pm 0.03 \times 10^{-6}$ cm^2 s^{-1}. These values are in good agreement with the literature data [27].

3.1.2. *Potentiostatic transients*

In Figures 8, 9 we report potentiostatic transients for prolonged electrodeposition from pure sulphate solutions and baths containing PEG and 500 ppm NaCl. Two broad classes of long-term behaviour can be noticed with both baths: either the transients tend to an approximately constant value (no PEG −100 and −200 mV, with PEG −100 to −300 mV) or they tend to diverge. At short times other types of transient can be noticed. Without PEG, at all investigated overpotential values, the c.d. always increases, either settling to a constant value or tending to diverge. With PEG this scenario can be observed only for voltages higher than −700 mV: at lower voltages the c.d. initially tends to

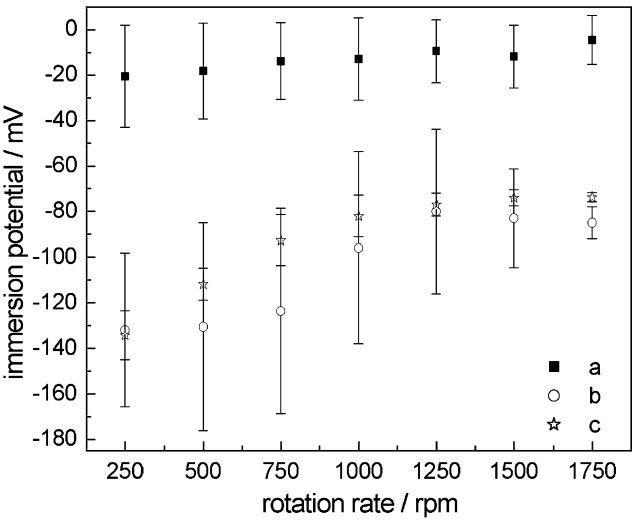

Fig. 7. Immersion potential ±1SD, estimated from the Butler-Volmer model (see Section 1.1), as a function of the RDE electrode rate for the solutions: (a) $CuSO_4{\cdot}5H_2O$ 20 mM and H_2SO_4 0.5 M, (b) $CuSO_4{\cdot}5H_2O$ 20 mM, H_2SO_4 0.5 M and PEG MW 1500 2 g l^{-1}, (c) $CuSO_4{\cdot}5H_2O$ 20 mM, H_2SO_4 0.5 M PEG MW 1500 2 g l^{-1} and NaCl 500 ppm.

decrease and afterwards either it settles to a constant value (−100 to −300 mV) or it increases again, eventually tending to diverge. The latter behaviour can be related to the development of unstable morphologies such as dendritic and loose granular. Nucleation phenomena can cause the initial portion of c.d. transients to be characterised either by the presence of a maximum (without PEG: −100 to −300 mV) or by a monotonic c.d. increase (without PEG: −500 mV and more cathodic, with PEG: −900 mV and more cathodic) [33]. The initial c.d. decrease observed in some transients in the presence of PEG, can be explained with the build up of a PEG-containing inhibiting layer.

In the literature, it was found that a critical overpotential η_{cr} exists for dendritic growth initiation [34, 35], lying within the limiting c.d. plateau. η_{cr} was shown to be directly proportional to j_{lim}/j_o or to h/ δ, where j_{lim} is the limiting c.d., j_o the exchange c.d., h the precursor height and δ the concentration boundary layer thickness. An induction period t_{cr} before initiation of dendritic growth was also demonstrated, during which dendrite precursors form and grow before attaining a dimension of the order of δ. The initiation of dendritic growth at time t_{cr} is denoted by a change in the slope of the log(j) vs t curves. The slope before dendritic growth inception – corresponding to non-dendritic electrode coarsening – is independent of the overpotential. After initiation of dendritic growth, the slope becomes a function of the overpotential. By plotting t_{cr} vs η and extrapolating to zero, t_{cr}, η_{cr} can be estimated. Departures from linearity can be found in our data and also in the literature [36], but these have not been commented upon. This behaviour can be linked to concurrent hydrogen evolution; in particular, the build-up of bubbles in the catholyte decreases the effective cathode area by a factor 0, which is a function of time and overpotential. The overpotential-dependent slope β for times exceeding t_{cr} can thus be tentatively written as:

$$\beta = d[\ln(j)]/dt = V/nF \cdot [j_o \theta \exp(\eta/B_c)/\delta]^2 \qquad (1)$$

where j is the nominal c.d. and θ a decreasing function of time.

The potentiostatic transients for the solution without PEG can be followed in Figure 8. The slopes β resulting from least-squares fitting of the linear regions, where they apply, and their 95% confidence intervals are reported in Figure 10. Good determination coefficients were found: $\rho^2 = 0.998 \pm 0.001$.

The low-overpotential transients (at −100 and −200 mV) reach asymptotic c.d.s in a few hundred seconds. At intermediate overpotentials (−300 and −500 mV) the potentiostatic transient shows two linear regions, as predicted by the dendritic growth theory of [34, 35], a transition time of about 2500 s can be estimated. For experiments in the high-overpotential range (−700 to −1300 mV) one can observe only one linear growth range, with sublinear behaviour for the highest times.

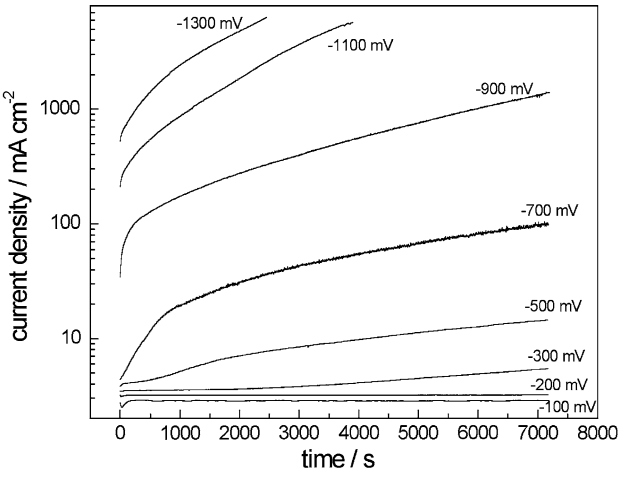

Fig. 8. Potentiostatic transients curve for electrodeposition from a solution containing $CuSO_4 \cdot 5H_2O$ 20 mM and H_2SO_4 0.5 M. Potentials reported vs Ag/AgCl.

The potentiostatic transients for the solution with PEG and NaCl are reported in Figure 9. The slopes resulting from least-squares fitting of the linear regions, where they apply, are reported in Figure 10. Good determination coefficients were obtained also in this case: $\rho^2 = 0.992 \pm 0.007$. Coherently with our CV results, sizably lower c.d. values are obtained in the presence of PEG. At low overpotentials (from −100 to −300 mV) a fast c.d. decrease can be noticed, followed by very slow c.d. decrease, possibly due to cathode passivation with suppressor-related species, eventually reaching an asymptote in a few hundred seconds. Occasional c.d. increases can be noticed extending over periods of some hundred seconds, possibly due to the rupture and healing of the inhibiting layer. At intermediate overpotentials (from −500 to −900 mV) a fast c.d. decrease is followed by an exponential c.d. increase. At overpotentials in

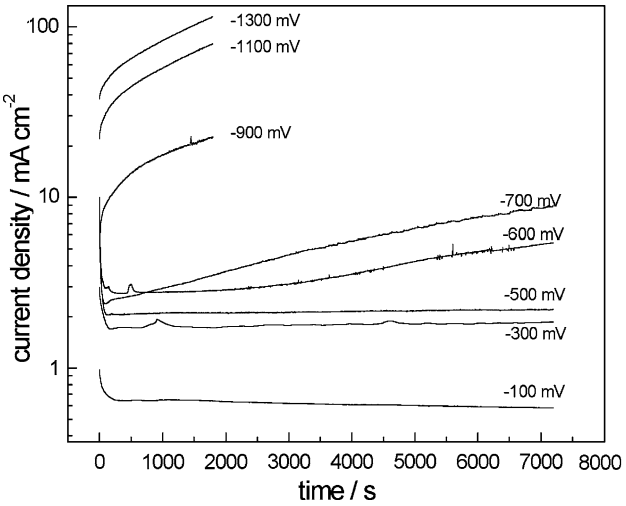

Fig. 9. Potentiostatic transients curve for electrodeposition from a solution containing $CuSO_4 \cdot 5H_2O$ 20 mM, H_2SO_4 0.5 M, PEG MW 1500 2 g l^{-1} and NaCl 500 ppm. Potentials reported vs. Ag/AgCl.

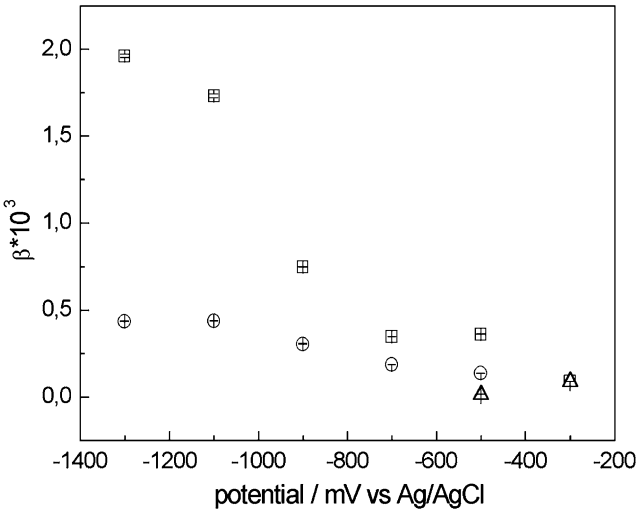

Fig. 10. β slopes and respective 95% confidence intervals (see Section 1.2) derived from the transients of Figures 8 and 9. Squares (short-time slopes) and triangles (long-time slopes): no PEG. Circles: with PEG.

excess of −1100 mV a smooth, approximately linear c.d. increase is noticed, followed by an exponential increase.

From the results of the potentiostatic transients it can be concluded that for the bath without PEG a critical overpotential for dendritic growth can be estimated of ca. −550 mV. In the presence of PEG an essentially potential-independent exponential c.d. divergence is observed, suggesting that critical overpotential and transition time are higher than those accessed by our experiments. This is coherent with our SEM observations of the growth morphologies.

3.1.3. *Cathodic efficiency*

Galvanostatic cathodic current efficiency (c.c.e.) measurements were carried out with soluble and insoluble anodes in the absence and in the presence of NaCl and PEG at 0.2 and 1.0 mA cm^{-2}. Experiments lasting 12 h each, were run in triplicates. After each electrodeposition run with the insoluble anode, the Cu^{2+} content is restored by dissolving a suitable amount of $CuSO_4 \cdot 5H_2O$ in the bath. The c.c.e. was estimated by weight gain measurements and with the assumption that Cu^{2+} is reduced to Cu metal. The relevant results are shown in Table 1 and discussed below.

(a) Experiments carried out at 0.2 mA cm^{-2} with a soluble anode exhibit c.c.e.s in excess of 100%, with a serial correlation across the experiments carried out on single days after letting the solution stand overnight. The c.c.e. thus tends to grow as plating time lapses, but it is reset to an initial value after ageing the bath.

(b) The c.c.e. measured in conditions different from (a) are invariably lower than 100%. Even if the confidence intervals for case (b) are rather broad, the data seem to suggest that the c.c.e.s are lower in the presence of PEG and both PEG and Cl^-.

(c) C.c.e.s with an insoluble anode are invariably lower than with a soluble one. The presence of PEG seems to give rise to a complex electrochemical behaviour, which can be explained with the stabilisation of Cu^+ produced at the soluble anode. Other plating additives were reported to increase the Cu^+ concentration in acid sulphate baths [37]. This effect is time-dependent; a build-up of Cu^+-containing species reaching the cathode seems to develop during the bath operation. The lability of Cu^+-complexes can derive either from the fact that reaction products of PEG show the relevant complexing ability or that such complexes are not stable against environmental oxidation to Cu^{2+}. This kind of behaviour seems to be absent at higher c.d.s, where the presence of PEG relates to lower c.c.e.s. This may be due to localised c.d. increase owing to partial cathode coverage with organic species and hydrogen evolution.

3.2. *Scanning electron microscopy of potentiostatic deposits*

In-plane SEM micrographs of thick (thickness in excess of 30 μm) Cu layers deposited potentiostatically in the absence and in the presence of PEG are shown in Figures 11–14 and 15–18, respectively. Amorphous Ni–P(9%) substrates were used, prepared as described in [38].

3.2.1. *Peg-free solution*

At low overpotentials (−100 and −200 mV) a compact and grainy morphology is obtained, with average

Table 1. Cathodic efficiency for the galvanostatic deposition of Cu from solutions without and with PEG and NaCl

	Soluble anode 0.2 mA cm^{-2}	Insoluble anode 0.2 mA cm^{-2}	Soluble anode 1.0 mA cm^{-2}	Insoluble anode 1.0 mA cm^{-2}
No additives	98.7 ± 0.9	98.3 ± 1.4	98.6 ± 2.2	98.5 ± 3.54
PEG	107.3 ± 2.5 1st run 114.3 ± 7.5 2nd run 136.1 ± 15.6 3rd run	96.6 ± 2.8	97.3 ± 4.0	83.5 ± 2.7
PEG + NaCl	98.5 ± 2.1 1st run 113.6 ± 6.4 2nd run 129.0 ± 7.1 3rd run	95.3 ± 4.6	96.7 ± 4.7	86.7 ± 1.2

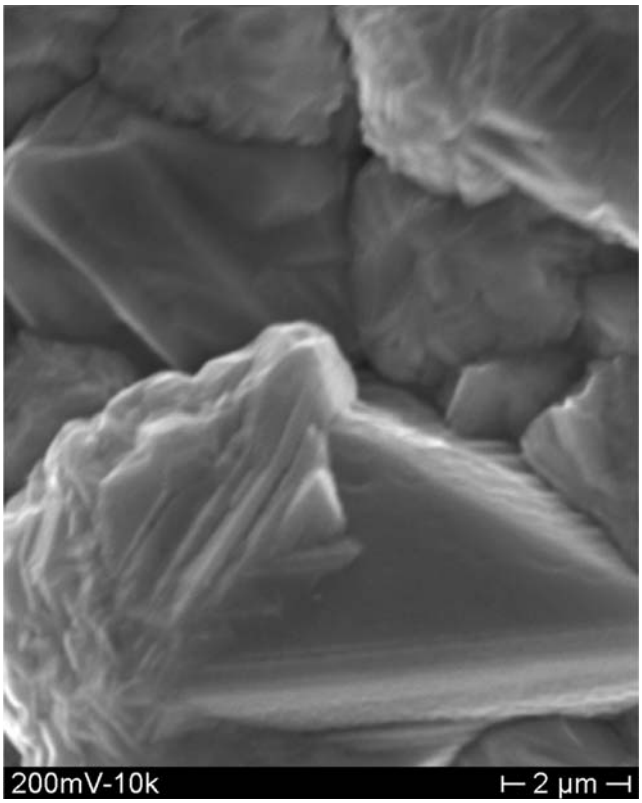

Fig. 11. SEM micrograph of Cu deposited from a solution containing $CuSO_4 \cdot 5H_2O$ 20 мм and H_2SO_4 0.5 м, obtained at −200 mV vs Ag/AgCl, magnification 10,000×.

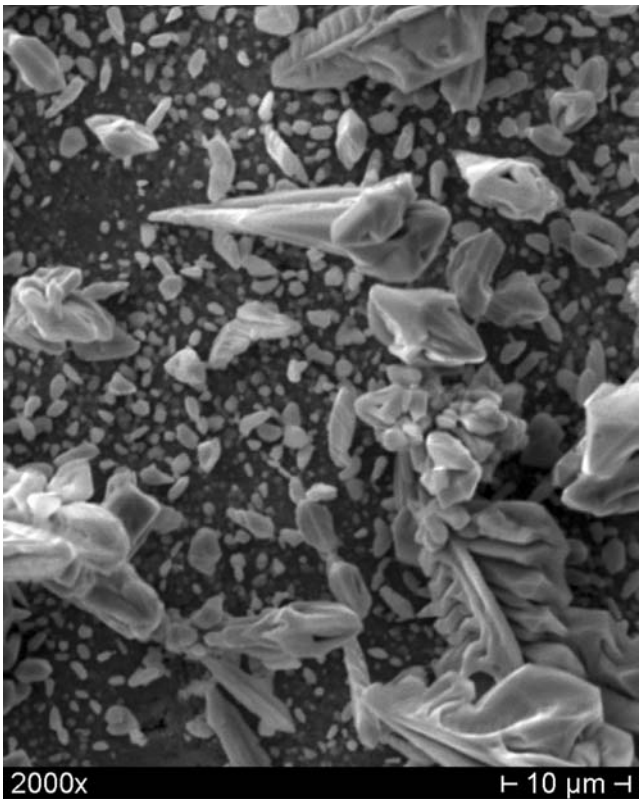

Fig. 12. SEM micrograph of Cu deposited from a solution containing $CuSO_4 \cdot 5H_2O$ 20 мм and H_2SO_4 0.5 м, obtained at −500 mV vs Ag/AgCl, magnification 2000×.

crystallite diameter of ca. 3 μm and a broad crystallite size distribution (ca.1 − −7 μm) (Figure 11). Crystallites characterised by stacking of macrosteps with square terraces and secondary nucleation can be observed. The overall morphology of typical crystallites seems dominated by twinning within the terraces, with a secondary contribution from renucleation onto growing crystallites. Smaller terrace stacks sometimes appear as globular features on well-developed crystallites. Additive-free acidic Cu sulphate baths exhibit relatively low crystallisation overpotentials and relatively high exchange c.d.s; the comparatively high deposition overpotentials employed in this research result in a vanishing nucleation-exclusion zone and an attendant large nucleation rate [12, 39–44]. At −200 mV some elongated crystallites appear, with a smooth aspect and ridges along the main dimension. Similar ridges have been sometimes observed in Cu electrodeposits, but not explained from a mechanistic point of view [42, 45]. In this case, however, square terraces are hardly observable; a reason for this can be the more extensive twinning due to higher overpotentials [46] – giving rise to poorly defined squares – and less obvious bunching. As a consequence, macrosteps are thinner and appear somehow blurred.

A dendritic morphology develops at −300 mV above a finely grained background. The prompt development of dendritic growth with amplification of surface irregularities characterised by high aspect ratios, actually gives

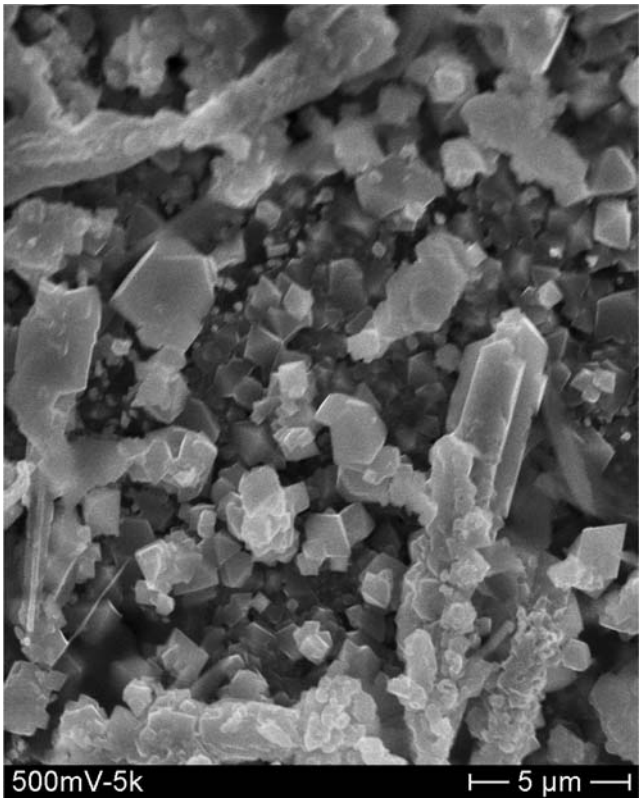

Fig. 13. SEM micrograph of Cu deposited from a solution containing $CuSO_4 \cdot 5H_2O$ 20 мм and H_2SO_4 0.5 м, obtained at −500 mV vs Ag/AgCl, magnification 5000×.

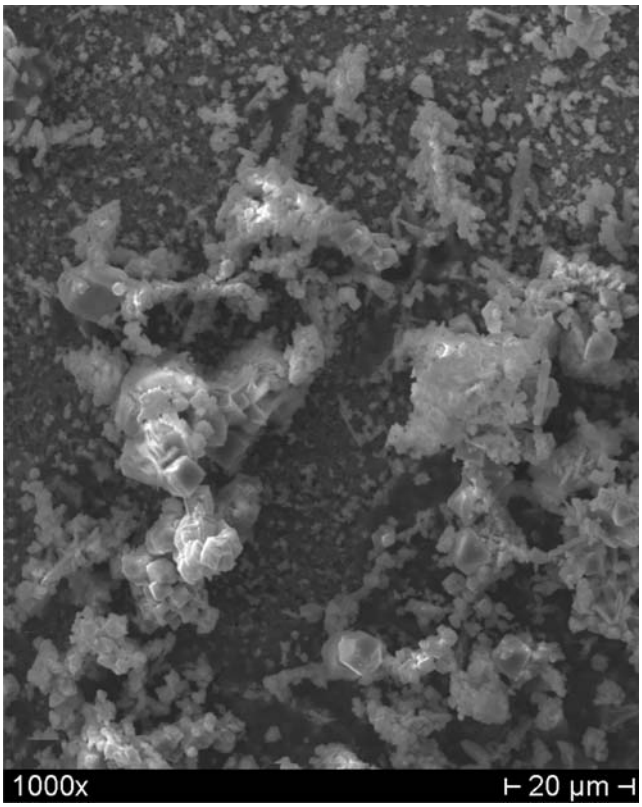

Fig. 14. SEM micrograph of Cu deposited from a solution containing $CuSO_4 \cdot 5H_2O$ 20 мм and H_2SO_4 0.5 м, obtained at −900 mV vs Ag/AgCl, magnification 1000×.

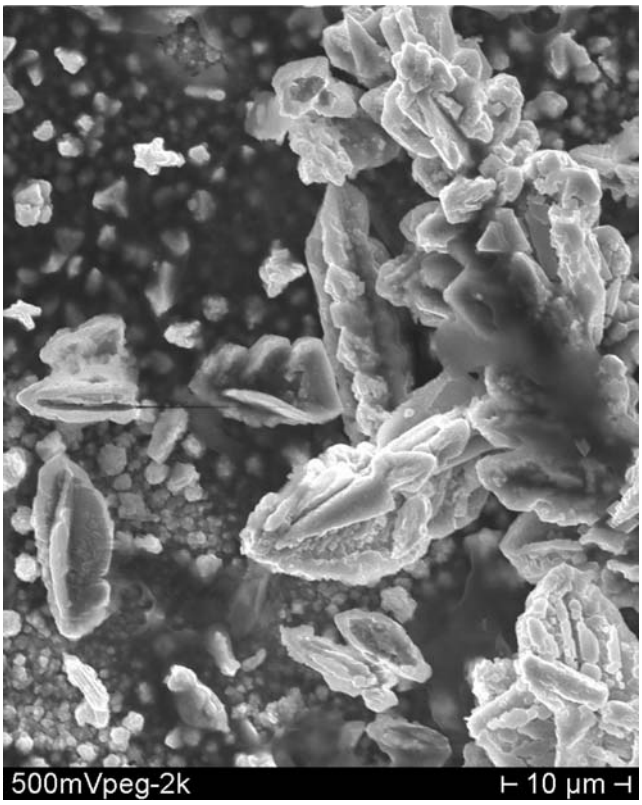

Fig. 16. SEM micrograph of Cu deposited from a solution containing $CuSO_4 \cdot 5H_2O$ 20 мм, H_2SO_4 0.5 м and PEG MW 1500 2 g l^{-1}, obtained at −200 mV vs Ag/AgCl, magnification 13,000×.

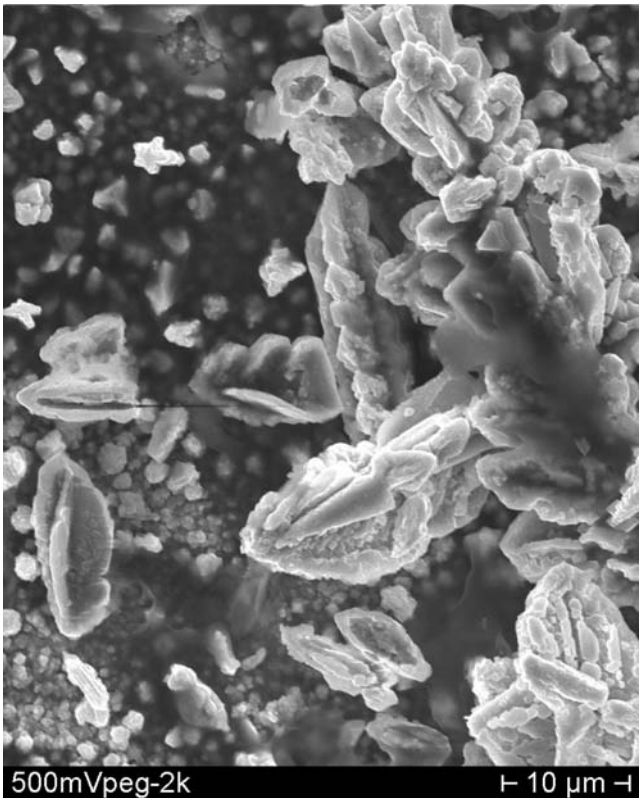

Fig. 15. SEM micrograph of Cu deposited from a solution containing $CuSO_4 \cdot 5H_2O$ 20 мм, H_2SO_4 0.5 м and PEG MW 1500 2 g l^{-1}, obtained at −500 mV vs Ag/AgCl, magnification 2000×.

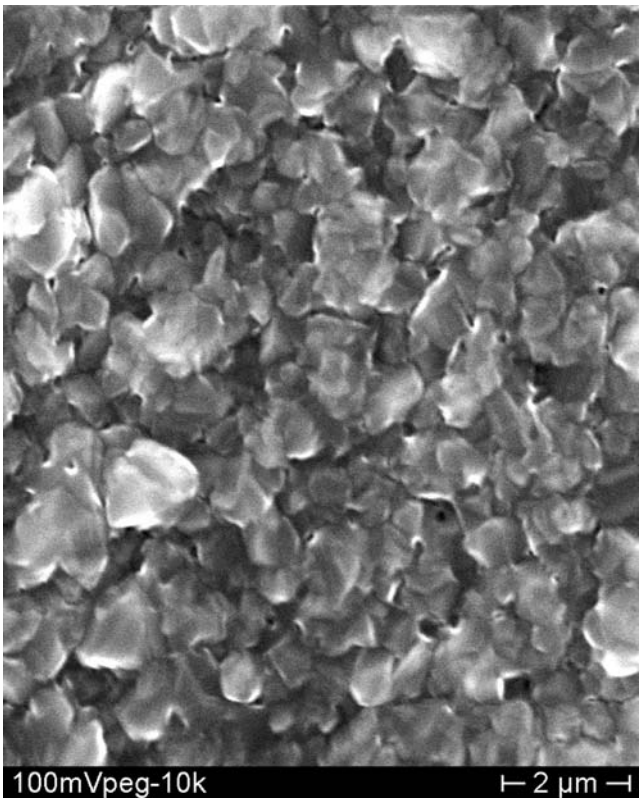

Fig. 17. SEM micrograph of Cu deposited from a solution containing $CuSO_4 \cdot 5H_2O$ 20 мм, H_2SO_4 0.5 м and PEG MW 1500 2 g l^{-1}, obtained at −100 mV vs Ag/AgCl, magnification 10,000×.

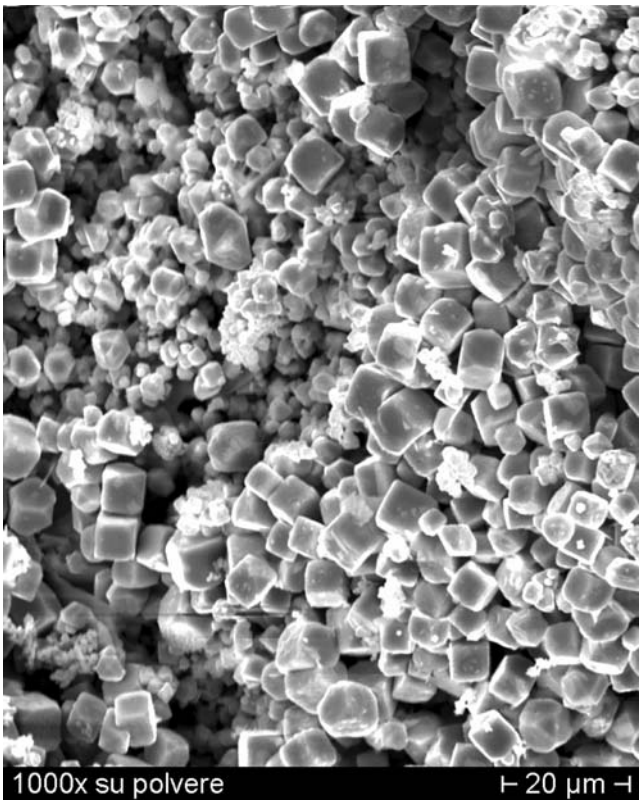

Fig. 18. SEM micrograph of Cu deposited from a solution containing $CuSO_4 \cdot 5H_2O$ 20 mM, H_2SO_4 0.5 M and PEG MW 1500 2 g l^{-1}, obtained at −500 mV vs Ag/AgCl, magnification 1000×.

rise to geometrical conditions that are compatible with the formation of nucleation-exclusion zones. Such features can be explained as follows: (a) dendritic growth conditions are operative, causing the formation of outgrowth features, (b) ridges form along the main dimension of the dendrites, (c) smoothness can be due to limited bunching related to the fact that the Cu surface is bare under the prevailing electrode conditions [40, 47, pp. 37–38].

Potentiostatic electrodeposition at −500 mV takes place in the presence of intense hydrogen evolution. Dendritic growth is apparently disrupted, possibly owing to increased catholyte stirring. A combination of growth features can be noticed at this voltage (Figure 12). (a) Unevenly distributed fine-grained globular crystallites form the background. In some regions these crystallites tend to cluster, giving rise to a morphology resembling the so-called spongy kind of disperse deposit [48]. Such features are typical for full diffusion-controlled electrodeposition conditions. (b) Well-developed crystallites with overall geometries relating to cubic crystal symmetry appear at some points of the deposit, this kind of growth form is typical for activation-controlled electrodeposition [41, 49]. Transition structures between cubic crystallites and needle-shaped features exhibiting an extension of the cubic structures appear, such features have been reported in the literature for acidic sulphate Cu electrodeposition in the range of activation-controlled electrode kinetics [49]. (c) Needle-shaped dendrite precursors; these features are typical of overpotential conditions close to critical for dendrite development. The simultaneous presence of all the above-mentioned morphological features suggests that different electrochemical conditions prevail at different locations of the electrode. This can be explained in terms of local screening effects deriving from the distribution of hydrogen bubbles at the electrode surface and in the catholyte. Like in the case of dendritic growth, the surface protrusions grow under activation control, while on the rest of the cathodes electrodeposition goes on predominantly under diffusion control [35]. Essentially the same qualitative comments apply for the potential range −500 to −1300 mV. At −500 mV, the fine-grained background exhibits some voids, which can be explained with the adhesion of hydrogen bubbles (Figure 13) [40, 50]. Similar features were observed by *ex situ* optical microscopy and AFM for acidic sulphate baths in the absence of organic additives [13]. An array of cubic crystallites interspersed with clusters of globular fine grains can be observed at −1300 mV, the deposit is loose and of the granular type [51]. Some crystallites exhibit very obvious twinning relationships between cubic sub grains

3.2.2. *Peg-containing solution*

The presence of PEG gives rise to remarkable grain-refining, coherently with the results of nucleation transients [13]. This can be appreciated in particular at the lower cathodic voltages (−100 to −300 mV) (Figures 16, 17). In the presence of PEG, the grain size distribution is narrower and the average diameter is ca. 1 μm, the grains exhibit a flaky, plate-like appearance, macrosteps cannot be detected with magnifications up to 13,000 ×. This result is coherent with *ex situ* field-effect scanning electron microscopy literature results revealing that PEG molecules adsorb preferentially at the edges of Cu macrosteps, thus inhibiting lateral growth [25]. No growth features are observed, which can be correlated to obvious crystallographic elements of fcc Cu. Strong growth inhibition can in fact even out the growth rates of the different crystal faces, giving rise to globular and smooth crystallites [52]. Spheroidal crystallites tend to develop, characterised by the presence of randomly distributed submicrometric ridges (Figure 16), which can be related to crystal planes deriving from renucleation on pre-existing crystallites [47, pp. 37–38] and possibly exhibiting twinning relationships [53]. Extensive macrotwinning in fact was reported for galvanostatic deposition from baths containing PEG in the absence of Cl^- [12]. At −300 mV some of the outgrowing globuli exhibit ridged structures, of the type noticed in the absence of PEG at −200 mV, and found to act as dendrite precursors. A similar morphological behaviour was observed with Ag after adding ammonium salts to a nitrate bath [54] and with Cd after addition of ethylene oxide [55], which was reported to adsorb at the cathode during growth.

Electrodeposits obtained at −500 mV in the presence of PEG exhibit dendritic growth (Figure 15). The dendrites developing in the PEG-containing system are remarkably more branched. A higher degree of branching can be related to lower field localisation conditions. In fact, owing to PEG adsorption, electrochemical conditions favourable to dendritic growth are present also along the dendrite stalk and not only at the tip. This kind of behaviour – which is related to the new-nucleation features observed at lower cathodic overpotentials – can be related to the cathodic presence of a suppressor, tending to even out the localisation of growth conditions. Further evidence of this behaviour can be derived from the fact that dendritic features observed at high magnification show branching precursors. This observation is consistent with the fact that the critical overpotential for the onset of dendritic growth is increased by the addition of PEG to the plating solution. Outgrowth features exhibiting pentagonal features appear (Figure 15) related to twinning [46]. Essentially the same morphology can be observed at higher cathodic overpotentials.

3.3. *In situ surface enhanced Raman spectroscopy*

Potential-dependent spectra obtained in the absence and in the presence of PEG are shown in Figures 19 and 20, respectively. Some faint vibrational features, related to bulk species appear in Figure 19, while obvious PEG-related bands show up in Figure 20. In Figure 19 we can observe bands at ca. 1200 and 1610 cm^{-1}. The band located at 1610 cm^{-1} is due to water bending. According to [56, 57] the inorganic sulphate ion absorbs strongly at 1200–1020 cm^{-1} (out-of-phase SO_4 stretching). At polarisations more negative than the Cu PZC (−200 mV in NaOH 0.1 M [31]), sulphate ions are expected to desorb. We therefore have reason to believe that these features derive from bulk species. Even though no surface vibrational bands can be measured under these conditions, it is known that the background derives from the surface enhancement effect and this, in turn, is related to the surface features developing during cathodic accretion. Therefore, the background level at a given Raman shift yields information on the electrocrystallisation process.

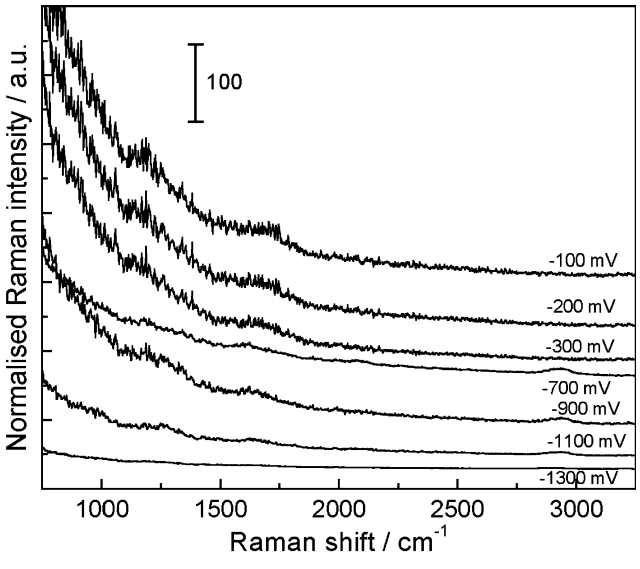

Fig. 19. In situ SERS spectra measured with a solution containing $CuSO_4 \cdot 5H_2O$ 20 mM and H_2SO_4 0.5 M. Potentials reported vs Ag/AgCl.

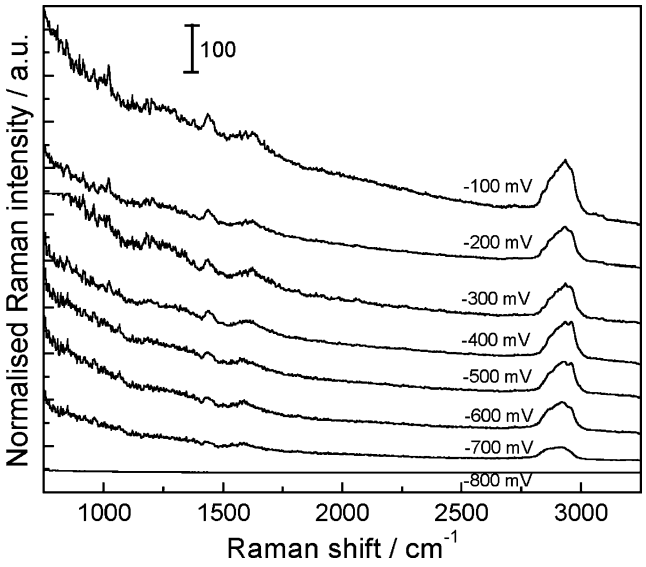

Fig. 20. In situ SERS spectra measured with a solution containing $CuSO_4 \cdot 5H_2O$ 20 mM, H_2SO_4 0.5 M and PEG 2 g l^{-1}. Potentials reported vs Ag/AgCl.

Comparing a typical SERS spectrum (from Figure 20) with the Normal Raman spectrum of PEG powder (Figure 21), we notice that some peaks can be related to traces of unreacted PEG and other ones to PEG reaction products. Even though the quality of the PEG-related SERS bands obtained during electrodeposition from acidic sulphate baths is not as high as during electrodeposition from cyanoalkaline solutions [58] or anodic attack of layers incorporating PEG [59], it

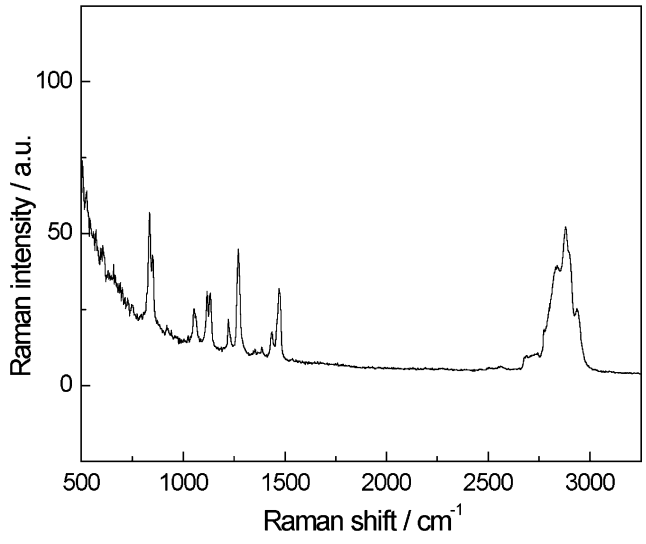

Fig. 21. Normal Raman spectrum of PEG powder.

is nevertheless acceptable for qualitative comments on adsorption during plating and spectral interpretation.

The list of the Raman bands observed in Figure 20 and their interpretation are reported below.

1020 cm^{-1} – C–O stretching of an aliphatic alcohol group.

1203 cm^{-1} – asymmetric stretching C–O–C of the vinyl ether group.

1440 cm^{-1} – CH_2 scissoring of the methylene groups in the molecule chain;

1631 cm^{-1} – C=C stretching in the vinyl group; in better-resolved galvanostatic spectra (Figure 22) this peak shows a well-defined doublet structure, which is typical for rotational isomers.

3082 cm^{-1} and 2900 cm^{-1} – symmetric and asymmetric stretching vibrations of the C–H bond in the $H_2C=$ groups and stretching of the C–H bond in the RHC= group.

The variation of the intensities and peak positions of these bands upon shifting the potential in the cathodic direction can be summarised as follows: (a) the intensity of the bands at 1020 and 3082 cm^{-1} decreases; (b) the intensity of the band at ca. 2900 cm^{-1} increases; (c) the intensity of the band at 1440 cm^{-1} is approximately constant. No shift of the band positions can be measured. This scenario is compatible with a decrease in the surface concentration of reacted vs unreacted PEG. The constancy of the band intensity around 1440 cm^{-1} might be explained with the fact that, owing to the shift in peak position brought about by PEG reaction, the poorly resolved broad band might contain contributions from both unreacted and reacted PEG, eventually giving rise to a constant intensity of the compound band. The intensity of the bands located at 1203 and 1631 cm^{-1} could be affected by the presence of electrolyte bands at nearby wavenumbers, associated with sulphate and water, respectively.

The peaks observed can be assigned to a vinyl ether group. The spectral differences between adsorbed PEG-related species and PEG powder can therefore be interpreted in terms of polymer fragmentation and further reaction of the fragmentation products. The gathered evidence is consistent with a reaction process involving ether bond cleavage at the electrode surface; the first step of the process can be a nucleophilic substitution, successive unimolecular or bimolecular elimination reactions could introduce the vinyl ether group in the substituted products. From these cathodic spectra, it can be concluded that PEG reaction takes place during electrodeposition.

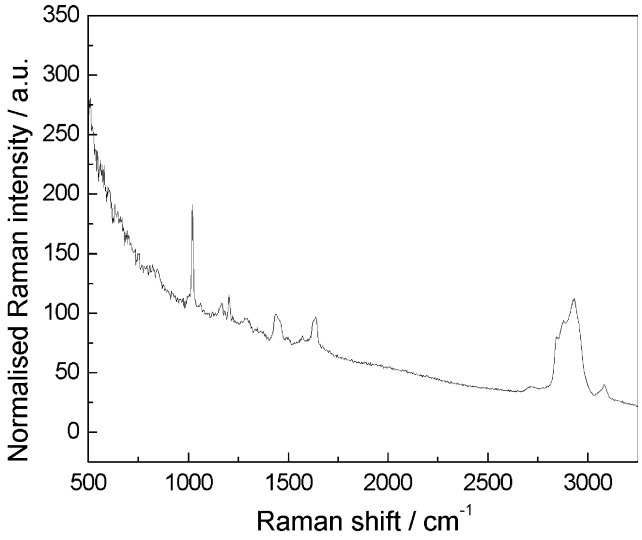

Fig. 22. In situ SERS spectra measured with a solution containing $CuSO_4 \cdot 5H_2O$ 20 mM, H_2SO_4 0.5 M and PEG 2 g l^{-1}, at 10 mA cm^{-2}.

4. Conclusions

From the experimental results reported in this paper, the following conclusions can be drawn.

(a) PEG complexes Cu(II), as shown by immersion potentials measured by CV; Cl^- effects are minor ones in this respect.

(b) PEG stabilises Cu(I), as revealed by cathodic current efficiency measurements; again, Cl^- effects are higher-order ones.

(c) Analysis of the cathodic Tafel slopes suggests that PEG tends to enhance electron transfer, the effect of Cl^- in this case is a major one; this result, together with rotation-rate effects on the exchange current density and Tafel slope in the presence of Cl^-, suggest that the adsorption mode of Cl^- is such that it acts as a spacer between the metal and the PEG layer.

(d) PEG is adsorbed during Cu electrodeposition, this explains suppressor activity; this conclusion is based on the following data:

(d1) exchange current density is decreased in the presence of PEG;

(d2) micrography shows that PEG gives rise to major grain refining effects (globular features are stabilised vs faceted ones), favours renucleation onto growing crystallites, delays dendrite formation and stabilises the growth of branched vs smooth dendrites;

(d3) potentiostatic transients prove that PEG increases the critical overpotential and transitions times to dendritic growth;

(d4) SERS measurements provide evidence of surface vibrational bands related to PEG and PEG reaction products.

(e) PEG reacts at the cathode, as suggested by: (e1) cathodic current efficiency measurements showing that the formation of labile Cu(I) complexes correlates with the presence of PEG, Cl^- effects being minor ones and (e2) SERS showing that new peaks are formed at the cathode, which can be assigned to a vinyl ether group.

Acknowledgements

This research is part of the "Cathodic Accretion Ruled by Layer Adsorption" Project of the Faculty of Engi-

neering, Lecce University. Expert assistance with electrochemical and spectroelectrochemical experiments is gratefully acknowledged to Mr. Francesco Bogani. Intensive assistance with data elaboration is gratefully acknowledged to Ms. Serena De Paolis and Ms. Stefania Lezzi.

References

1. A. Damjanovic, T.H.V. Setty and J.O'M. Bockris, *J. Electrochem. Soc.* **113** (1966) 429.
2. H. Todt, *Galvanotechnik* **58** (1967) 852.
3. L. Mirkova and S. Rashkov, *J. Appl. Electrochem.* **24** (1994) 420.
4. U. Bertocci, *Electrochim. Acta* **11** (1966) 1261.
5. Z. Nagy, J.B. Blaudeau, N.C. Hung, L.A. Curtiss and D.J. Zurawski, *J. Electrochem. Soc.* **142** (1995) L87.
6. F. Texier, L. Servant, J.L. Bruneel and F. Argoul, *J. Electroanal. Chem.* **446** (1998) 189.
7. J.P. Healy, D. Pletcher and M. Goodenough, *J. Electroanal. Chem.* **338** (1992) 167.
8. G.A. Hope and G.M. Brown, Electrochemical Society Proceedings vol. 96–8, (1996) pp. 215–226.
9. J.D. Reid and A.P. David, *Plat. Surf. Fin.* **74** (1987) 66.
10. M.R.H. Hill and G.T. Rogers, *J. Electroanal. Chem.* **86** (1978) 179.
11. J.P. Healy, D. Pletcher and M. Goodenough, *J. Electroanal. Chem.* **338** (1992) 155.
12. A. Vicenzo and P.L. Cavallotti, *J. Appl. Electrochem.* **32** (2002) 743.
13. L. Bonou, M. Eyraud, R. Denoyel and Y. Massiani, *Electrochim. Acta* **47** (2002) 4139.
14. M. Yokoi, S. Konishi and T. Hayashi, *Denki Kagaku (English edition)* **52** (1984) 218.
15. D. Stoichev, I. Vitanova, St. Rashkov and T. Vitanov, *Surf. Technol.* **7** (1978) 427.
16. J.J. Kelly and A.C. West, *J. Electrochem. Soc.* **145** (1998) 3472.
17. J.J. Kelly and A.C. West, *J. Electrochem. Soc.* **145** (1998) 3477.
18. J.J. Kelly, C. Tian and A.C. West, *J. Electrochem. Soc.* **146** (1999) 2540.
19. T.P. Moffat, J.E. Bonevich, W.H. Huber, A. Stanishevsky, D.R. Kelly, G.R. Stafford and D. Josell, *J. Electrochem. Soc.* **147** (2000) 4524.
20. P. Taephaisitphongse, Y. Cao and A.C. West, *J. Electrochem. Soc.* **148** (2001) C492.
21. J.J. Point and P. Damman, *Macromolecules* **25** (1992) 1184.
22. D. Suryanarayana, P.A. Narayana and L. Kevan, *Inorg. Chem.* **2** (1983) 474.
23. D. Stoichev and C. Tsvetanov, *J. Appl. Electrochem.* **26** (1996) 741.
24. J. Pearson and J.K. Dennis, *Surf. Coat. Technol.* **42** (1990) 69.
25. K. Kondo, N. Yamakawa, Z. Tanaka and K. Hayashi, *J. Electroanal. Chem.* **559** (2003) 137.
26. E. Gileadi, *Electrode kinetics* (VCH Publishers Inc., NY, 1993), 87 pp.
27. E.E. Farndon, F.C. Walsh and S.A. Campbell, *J. Appl. Electrochem.* **25** (1995) 574.
28. T.C. Franklin, *Surf. Coat. Technol.* **30** (1987) 415.
29. T.C. Franklin, *Plat. Surf. Fin.* **4** (1994) 62.
30. B. Bozzini, C. Mele, A. Fanigliulo, B. Busson, F. Vidal and A. Tadjeddine, *J. Electoanal. Chem.* **574** (2004) 85.
31. J. Koryta, J. Dvorak, L. Kavan, Principles of electrochemistry (Wiley, Chichester, 1993) 210 pp.
32. B. Bozzini and A. Fanigliulo, *J. Appl. Electrochem.* **32** (2002) 1043.
33. B.R. Scharifker and J. Mostany. *in* E.J. Calvo (Ed), Bard–Stratmann Encyclopaedia of Electrochemistry Vol 2, Interfacial kinetics and mass transport, (Wiley-VCH, Weinheim (D), 2003), pp. 512.
34. A. Despic and K. Popov. *in* R.E. White, B.E. Conway and J.O'M. Bockris (Eds), Modern Aspects of Electrochemistry 7, (Plenum Press, NY, 1972), pp. 264.
35. K. Popov, N. Krstajic and M. Cekerevac. *in* R.E. White, B.E. Conway and J.O'M. Bockris (Eds), Modern Aspects of Electrochemistry 30, (Plenum Press, NY, 1996), pp. 113.
36. K.I. Popov, M.D. Maksimovic, J.D. Trnjancev and M.G. Paunovic, *J. Appl. Electrochem.* **11** (1981) 239.
37. L.S. Melnicki, *in* L. Romankiw, T. Osaka (Eds) Electrochemical Technology in Electronics. ECS Proc Series PV 88–23, Pennington, NJ, 95 pp.
38. B. Bozzini, C. Lenardi, M. Serra and A. Fanigliulo, *Br. Corros. J.* **37** (2002) 173.
39. W.S. Kruijt, M. Sluyters-Rehbach, J.H. Sluyters and A. Milchev, *J. Electroanal. Chem.* **371** (1993) 13.
40. H. Seiter, H. Fischer and L. Albert, *Electrochim. Acta.* **2** (1960) 97.
41. S.C. Barnes, G.G. Storey and H.J. Pick, *Electrochim. Acta* **2** (1960) 195.
42. J.O'M. Bockris. *in* J.O'M. Bockris and B.E. Conway (Eds), Modern Aspects of Electrochemistry. Vol. 3, (Butterworths, London, 1964), pp. 261.
43. G. Wranglén, *Electrochim. Acta* **2** (1960) 130.
44. Paunovic M., Schlesinger M. (1998) Fundamentals of electrochemical deposition. Jonh Wiley and Sons, NY, pp 119–121.
45. T.B. Vaughan and H.J. Pick, *Electrochim. Acta* **2** (1960) 179.
46. V.M. Kozlov and L. Peraldo Bicelli. *in* H.S. Nalwa (Ed), Handbook of Thin Film Materials. Vol. 1, (Academic Press, NY, 2002), pp. 559.
47. K.I. Popov, S.S. Djokic, B.N. Grgur, Fundamental Aspects of Electrometallurgy (Kluwer, NY, 2002) pp. 37–38, pp. 84–87.
48. K.I. Popov and N.V. Krstajic, *J. Appl. Electrochem.* **13** (1983) 775.
49. K.I. Popov, M.G. Pavlovic, Lj.J. Pavlovic, M.I. Cekerevac and G.Z. Remivic, *Surf. Coat. Technol.* **34** (1988) 355.
50. B. Bozzini, E. Griskonis, A. Fanigliulo and A. Sulcius, *Surf. Coat. Technol.* **154** (2002) 294.
51. A.T. Dimitrov, S. Hadzi-Jordanov, K.I. Popov, M.G. Pavlovic and V. Radmilovic, *J. Appl. Electrochem.* **28** (1998) 791.
52. B. Bozzini, A. Fanigliulo and M. Serra, *J. Crystal Growth* **231** (2001) 589.
53. B. Bozzini, P.L. Cavallotti, M. Ivanov, L. Arras, S. Garbarino, E. Terrenzio and P. Visigalli, *IEEE Trans. Magn.* **26** (1990) 45.
54. K.I. Popov, N.V. Krstajic and S.R. Popov, *Surf. Technol.* **20** (1983) 203.
55. K.I. Popov, Z.P. Rodaljevic, N.V. Krstajic and S.D. Novakovic, *Surf. Technol.* **25** (1985) 217.
56. N.B. Colthup, L.H. Daly, Introduction to Infrared and Raman Spectroscopy (Academic Press, Boston, 1990) 376 pp.
57. T. Iwasita and F.C. Nart. *in* H. Gerischer and C.W. Tobias (Eds), Advances in Electrochemical Science and Engineering, (Weinheim, VCH, 1995), pp. 123.
58. B. Bozzini, L. D'Urzo, C. Mele, Electrodeposition of Cu from cyanoalkaline solutions in the presence of cetylpyridinium chloride and poly(ethylene glycol): an electrochemical and in-situ SERS investigation. J. Electrochem. Soc. **152** (2005) C255.
59. B. Bozzini, L. D'Urzo, G. Giovannelli, C. Mele, An *in situ* Raman investigation of organic species incorporated in Cu layers electrodeposited from PEG-containing acidic sulphate and cyanoalkaline electrolytes. Trans. Inst. Metal Finish. **82** (2004) 118.